580 J. Med. Chem. 2011, 54, 580–590
DOI: 10.1021/jm101150b

Journal of Medicinal Chemistry Article

Structure-Based Design of Potent and Selective 2-(Quinazolin-2-yl)phenol Inhibitors of Checkpoint Kinase 2

John J. Caldwell,*,† Emma J. Welsh,† Cornelis Matijssen,† Victoria E. Anderson,† Laurent Antoni,† Kathy Boxall,† Frederique Urban,† Angela Hayes,† Florence I. Raynaud,† Laurent J. M. Rigoreau,§ Tony Raynham,§ G. Wynne Aherne,† Laurence H. Pearl,‡,∥ Antony W. Oliver,‡,∥ Michelle D. Garrett,† and Ian Collins†

†*Cancer Research UK Cancer Therapeutics Unit, The Institute of Cancer Research, 15 Cotswold Road, Sutton, Surrey SM2 5NG, U.K.,* ‡*Section of Structural Biology, Chester Beatty Laboratories, The Institute of Cancer Research, 237 Fulham Road, London SW3 6JB, U.K., and* §*Cancer Research Technology Discovery Laboratories London, Wolfson Institute for Biomedical Research, The Cruciform Building, Gower Street, London WC1E 6BT, U.K.* ∥*Present address: Genome Damage and Stability Centre, Science Park Road, University of Sussex, Falmer, Brighton, East Sussex, BN1 9RQ, U.K.*

Received September 6, 2010

Structure-based design was applied to the optimization of a series of 2-(quinazolin-2-yl)phenols to generate potent and selective ATP-competitive inhibitors of the DNA damage response signaling enzyme checkpoint kinase 2 (CHK2). Structure−activity relationships for multiple substituent positions were optimized separately and in combination leading to the 2-(quinazolin-2-yl)phenol **46** (IC_{50} 3 nM) with good selectivity for CHK2 against CHK1 and a wider panel of kinases and with promising in vitro ADMET properties. Off-target activity at hERG ion channels shown by the core scaffold was successfully reduced by the addition of peripheral polar substitution. In addition to showing mechanistic inhibition of CHK2 in HT29 human colon cancer cells, a concentration dependent radioprotective effect in mouse thymocytes was demonstrated for the potent inhibitor **46** (CCT241533).

Introduction

DNA damage in cells by external agents such as ionizing radiation or genotoxic chemotherapy leads to an accumulation of defective genetic material, which in turn can lead to tumorigenesis or apoptosis.[1,2] The typical cell cycle response to DNA damage involves activation of signal transduction pathways resulting in cell cycle arrest, proceeding to apoptosis or activation of repair mechanisms depending on the severity of the damage.[3,4] One key transducer of this DNA damage response is checkpoint kinase 2 (CHK2[a]), a serine/threonine kinase, which is activated in response to double-strand breaks in DNA.[5−9] Activation of the DNA damage sensor ataxia telangiectasia mutated (ATM) kinase in the presence of double-strand breaks results in phosphorylation of inactive CHK2 at Thr68.[10,11] Consequent homodimerization of CHK2 induces trans-autophosphorylation of Thr383 and Thr387, giving the fully activated enzyme, followed by cis-autophosphorylation on Ser516.[12−15] Activated CHK2 kinase has been found to be involved in a number of cell cycle events, including cell cycle arrest, apoptosis, DNA repair, and mitosis.[3,5,16,17]

The involvement of CHK2 in multiple cell cycle and DNA repair processes has made evaluation of the kinase as a potential anticancer drug target difficult,[6] however, several possible therapeutic contexts for CHK2 inhibition have been suggested. In particular, the continuing use of DNA-damaging cancer treatment modalities has prompted exploration of CHK2 inhibition within this context.[18−23] Many tumors bypass normal cell cycle responses to DNA damage as a result of defective p53 tumor suppressor function.[24] In normal cells, p53 is activated by CHK2 and other kinases in response to double-strand DNA damage resulting in G1 cell cycle arrest and apoptosis.[25] Therefore, it could be expected that subsequent to a DNA damaging event, survival of normal cells could be enhanced through CHK2 inhibition. The validity of this approach has been tested by exposure of $chk2^{-/-}$ transgenic mice to ionizing radiation, which showed an increased resistance to apoptosis.[9,26] A radioprotective effect of CHK2 inhibition has also been demonstrated in isolated mouse thymocytes as well as human lymphocytes.[18,20] A further potential use of a CHK2 inhibitor within a clinical context has been suggested by the observation that depletion of CHK2 by siRNA increases cancer cell sensitivity to poly(ADP ribose)polymerase (PARP) inhibition.[45]

Single-agent inhibition of CHK2 may also provide an antitumor effect in cancer cells, and therefore a therapeutic approach, where CHK2 is highly activated, suggesting an essential role for survival.[6,16,17] Pommier et al. recently demonstrated antiproliferative activity of the small molecule CHK2 inhibitor PV1019 (**2**, Figure 1) as well as CHK2 siRNA in cancer cell lines with high intrinsic CHK2 expression.[27] Compound **2** also demonstrated in vitro potentiation of the DNA-damaging chemotherapeutics topotecan and camptothecin in OVCAR-4 and OVCAR-5 human tumor cells. However, the generality of potentiation of DNA-damaging agents by CHK2 inhibitors remains controversial[6,16,17] because other pharmacological inhibitors of CHK2, such as VRX0466617 (**1**, Figure 1), have not shown such effects.[20,22]

*To whom correspondence should be addressed. Phone: +44 207 352 8133 ext 4705. Fax: +44 208 722 4126. E-mail: john.caldwell@icr.ac.uk.

[a] Abbreviations: ATM, ataxia and telangiectasia mutated; CHK1, checkpoint kinase 1; CHK2, checkpoint kinase 2; DELFIA, dissociation-enhanced lanthanide fluorescent immunoassay; hERG, human ether-a-go-go related gene; PAMPA, parallel artificial membrane permeability assay.

 Published on Web 12/27/2010

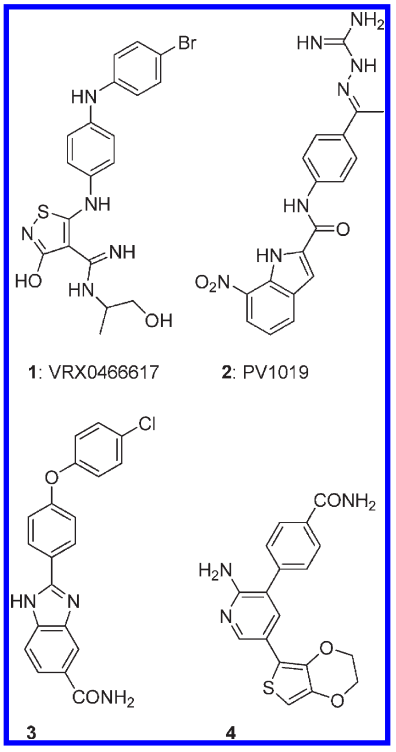

Figure 1. Reported ATP competitive, selective CHK2 inhibitors **1**−**4**.

A small group of ATP-competitive, selective CHK2 inhibitors have been reported in the literature thus far (Figure 1) based around isothiazoles **1**,[20,21] guanylhydrazones **2**,[22,27] and 2-arylbenzimidazoles **3**.[18,19] We have recently reported the identification of 2-aminopyridines, such as **4**, as CHK2 inhibitors.[23] The discovery of further CHK2 selective inhibitors and characterization of their pharmacology is important to elucidate the consequences and therapeutic utility of CHK2 inhibition in cancer. In particular, the separation of CHK2 activity from inhibition of the distinct DNA damage response signaling enzyme CHK1 is desirable to understand the phenotype of CHK2 inhibition with small molecules.[6] During kinome profiling of early hits from an unrelated kinase screening program, compounds containing the 2-(quinazolin-2-yl)phenol moiety were identified as potential CHK2 inhibitors.[28−30] Here, we report a structure-based approach to the optimization of novel 2-(quinazolin-2-yl)phenols to potent, selective CHK2 inhibitors and demonstrate their activity in cancer and nontumorigenic cell lines.

Results and Discussion

Screening of a small library of 2-(quinazolin-2-yl)phenols identified **5** (Table 1) as a starting point for the development of potent, selective quinazoline CHK2 inhibitors. As initial attempts to crystallize **5** bound to the CHK2 enzyme proved fruitless, synthetic efforts were first directed toward varying the amine substituent at the 4-position to gain potency and aid crystallization attempts. To this end, a range of acyclic aliphatic diamines were attached, however, no increase in CHK2 potency was found. The use of cyclic bis-amines connected through an exocyclic nitrogen to the quinazoline core led to greater success (Table 1). Specifically, (*S*)-pyrrolidine **10** gave a 10-fold improvement in potency relative to **5** and was also found to be 30-fold more active than the (*R*)-enantiomer **11**. Comparable potency to **10** was observed with the

Table 1. Investigation of Cyclic 4-Amino Substitution and Phenolic Substitution

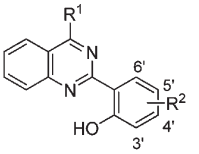

No.	R^1	R^2	CHK2 IC_{50} (μM) [a]
5		H	1.5
6	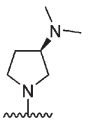	3'-F	>100
7		4'-F	1.69 (1.75, 1.63)[b]
8		5'-F	0.86 (0.56, 1.17)[b]
9		6'-F	5.4 (3.78, 7.01)[b]
10	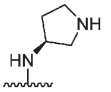	H	0.16 (0.14, 0.18)[b]
11	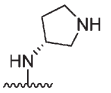	H	5.1
12	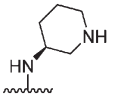	H	1.3
13	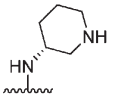	H	0.18 (±0.04)[c]
14	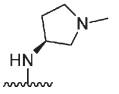	H	0.92 (±0.33)[c]
15	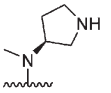	H	0.50 (0.65, 0.34)[b]
16	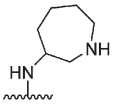	H	0.25 (±0.07)[c]
17	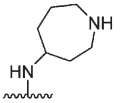	H	0.51 (0.60, 0.42)[b]

[a] Single determination in DELFIA assay format unless otherwise noted. Standard inhibitor staurosporine gave mean (±SEM) IC_{50} = 27 (±2.6) nM, n = 10. [b] Mean of n = 2 determinations, individual values in parentheses. [c] Mean (±SEM), n = 3.

(*R*)-piperidine **13**, although for the six-membered ring, the (*R*)-stereochemistry was favored over the (*S*)-enantiomer **12**. The racemic 3-aminoazepine **16** was similarly active, although a slight drop in activity was noted when the alternative 4-aminoazepine was introduced in **17**, indicating a preference for a constrained two-atom spacer between the two nitrogens. The secondary nature of both the ring and exocyclic nitrogens was shown to be important by the fall in activity of the *N*-methylated compounds **14** and **15** compared to the unsubstituted analogue **10**.

Further development of structures based around **10** appeared promising, given both the availability and synthetic tractability of 3-aminopyrrolidine intermediates. Importantly,

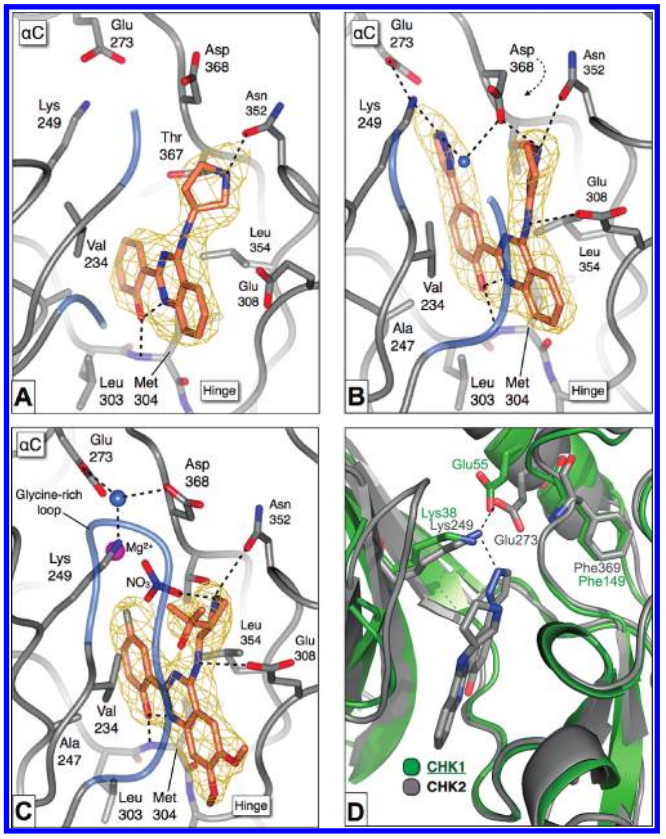

Figure 2. Molecular details for the binding of (A) **10** (PDB 2XM8), (B) **24** (PDB 2XM9), (C) **46** (PDB 2XBJ) to CHK2 (gray, C-α backbone "tube"). Nitrogen, oxygen, and fluorine atoms are colored blue, red, and gray, respectively. Blue spheres represent water molecules, and magenta spheres a magnesium ion. Residues of the glycine-rich loop, when ordered, are indicated by the transparent blue section of backbone "tube". Ligands, in each case, are shown in "stick" representation, with carbon atoms colored orange. Representative electron density from omit maps are shown in each case by the "chicken-wire" mesh, contoured at 1.4 (A) or 2.5 (B,C) σ. (D) Pymol overlay of the crystal structure of **24** in CHK2 (gray) with that of CHK1 (green; PDB 2C3I). Dashed lines represent hydrogen bonds formed by the CHK2 side chains Lys240 and Glu273 to the pyrazole. Parts (A−C) were produced using CCP4MG.[44]

we were able to obtain the crystal structure of **10** complexed with CHK2 (Figure 2, PDB 2XM8). This showed that **10** bound within the ATP pocket of the enzyme, with an intramolecular hydrogen bond present between the phenolic hydrogen and the quinazoline N-1, forming a planar, pseudotetracyclic core scaffold. The quinazoline was sandwiched between the lipophilic side chains of Val234 and Leu354, with the side chains of Ala247, Leu301, and Leu303 also contributing to a hydrophobic surface surrounding the core. An intermolecular hydrogen bond was formed between the phenol oxygen and the amide NH of Met304 in the hinge region of the kinase, while the 6- and 7-positions of the quinazoline were directed toward the solvent exposed part of the enzyme. The pendant 3-aminopyrrolidine group occupied the ribose pocket, with the protonated pyrrolidine nitrogen forming a charge-assisted hydrogen bond with the side chain carbonyl of Asn352. The exocyclic nitrogen of **10** was close to the side chain of Glu308. In subsequent structures solved, the equivalent exocyclic nitrogen in other analogues was observed to form a charge-assisted hydrogen bond to this residue (Figure 2B,C). These interactions are consistent with the observed structure−activity (Table 1), where *N*-methylation of either nitrogen was found to be unfavorable and the two-carbon distance between the two nitrogens was optimal.

Concurrent with the studies on the amine group, substitution of the phenol group of **5** was investigated through the synthesis of a sequence of molecules containing fluorine at all positions around the ring (**6**−**9**, Table 1). Whereas fluoro-substitution at the 3′- and 6′-positions resulted in lower CHK2 inhibition, the 4′-fluoro substituent **7** was tolerated and the 5′-fluoro substituent **8** increased the activity by 2-fold. This structure activity was also consistent with the binding mode of the quinazoline shown for **10**, where the 5′-position on the phenolic ring appeared to offer most opportunity for further substitution. A fall in activity from substitution at the 3′-position would be expected due to close proximity to the wall of the binding pocket. Substitution at the 6′-position may be unfavorable due to repulsion between the fluorine and quinazoline N-3, disrupting the planar conformation of the core scaffold.

The (*S*)-3-aminopyrrolidine template of **10** was used as the core group for optimization of the 5′-substituent of the phenol. Replacement of the 5′-proton with fluorine gave a 3-fold improvement in potency with **18**, also observed with the chloride **19** (Table 2). A counterscreen of **18** against the CHK1 enzyme showed 17-fold selectivity for CHK2 relative to CHK1. As some 2-(quinazolin-2-yl)phenols have been reported as ligands for voltage-gated ion channels,[32] an early indication of potential hERG activity within the series was sought.[31] Compound **18** inhibited the hERG ion channel tail current by 90% at a concentration of 10 μM, which when titrated equated to an IC_{50} of 3 μM. It therefore became necessary to evaluate and to reduce this undesirable activity during further optimization of the series.[33]

Introduction of a small alkyl group at the 5′-position was tolerated, as in the methyl and trifluoromethyl analogues **20** and **22**, however, activity decreased with larger lipophilic groups such as isopropyl (**21**). From a range of five-membered heterocycles added to replace the 5′-alkyl substituent, the most significant improvement in activity relative to **10** was seen with the addition of a 4- or 3-pyrazole substituent, **23** and **24**, reaching low nanomolar activity against the CHK2 enzyme in the instance of **24**. We have previously shown the potential for pyrazole substituents to interact productively with the conserved catalytic residues within other protein kinases.[47] Interestingly, improved relative selectivity against CHK1 was observed for the pyrazol-3-yl isomer **24**. A further benefit of the pyrazole substituent was a reduction in hERG inhibition to levels comparable to those of DMSO control for **23**, while **24** showed a hERG IC_{50} of 16 μM (Table 2).

The crystal structure of **24** bound to CHK2 is shown in Figure 2B (PDB 2XM9). An additional interaction between the pyrazole and Lys249 was observed and is likely to account for the increase in CHK2 potency when compared to **10**, although a similar improvement in potency was surprisingly not seen for 4-pyrazole **23**.

In relation to the selectivity observed for **24**, the similarities between CHK2 and CHK1 were demonstrated by a sequence alignment (see Supporting Information) showing the highly conserved nature of the ATP-binding pockets when comparing the two enzymes. Surrounding the pocket, 10 out of 12 residues are identical, with the remaining two differing only by single methyl substituents. In an attempt to rationalize the improved selectivity of **24** for CHK2 over CHK1, the crystal structure of **24** bound to CHK2 was overlaid with a reported CHK1 structure (PDB 2C3I)[34] using Pymol[35] and assuming a

Table 2. Optimization of the Phenol Substituent

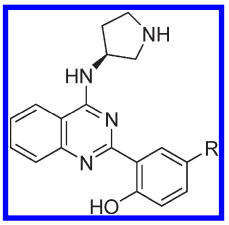

no.	R	CHK2 IC_{50} (μM)[a]	CHK1 IC_{50} (μM)[b]	CHK2/1 selectivity	hERG (inh@10 μM) (%)[c]
10	H	0.16 (0.14, 0.18)	4.5 (4.2, 4.7)	28	nd[d]
18	−F	0.060 (0.07, 0.05)	0.99 (1.2, 0.78)	17	90
19	−Cl	0.070 (0.11, 0.03)	nd	nd	nd
20	−Me	0.092 (±0.023)[e]	nd	nd	nd
21	$-^{i}$Pr	1.7[f]	nd	nd	nd
22	$-CF_3$	0.201 (±0.078)[e]	1.32 (1.30, 1.35)	7	96
23	pyrazol-4-yl	0.065 (0.079, 0.050)	1.91 (2.56, 1.25)	29	9
24	pyrazol-3-yl	0.009 (0.006, 0.012)	1.07 (1.1, 1.05)	119	23

[a] Two independent determinations in DELFIA assay format, individual values in parentheses. Standard inhibitor staurosporine gave mean (±SEM) IC_{50} = 27 (±2.6) nM, n = 10. [b] Two independent determinations in DELFIA assay format, individual values in parentheses. Standard inhibitor staurosporine gave mean (±SEM) IC_{50} = 2.1 (±0.41) nM, n = 26. [c] Mean of multiple determinations (n = 2−8) in a high-throughput cell-based electrophysiology assay for inhibition of hERG tail current.[31] DMSO 0.3% aqueous vehicle negative control gave 9−20% inhibition. One μM cisapride positive control gave 89−99% inhibition. [d] nd = not determined [e] Mean (±SEM) for n = 3 determinations. [f] n = 1 determination.

comparable hinge-binding mode for the inhibitor (Figure 2D). Close overlapping of the sequences with only minor changes in the positioning of the Glu-Lys salt bridge was seen. However, without the corresponding crystal structure of **24** in CHK1, analysis of such subtle structural differences, and whether they are significant, is difficult. A comparison of the crystal structures of the inhibitor debromohymenialdesine bound to both CHK2 and CHK1 has been included in the Supporting Information. Again, this shows similar differences to those shown in Figure 2D, with a 2.0 Å elongation of the Lys-Glu salt bridge observed. It remains to be seen if these small differences do indeed account for the difference in selectivity of **24** for CHK2 over CHK1. However, the improvement in selectivity observed for **24** does suggest that differences in this region of the CHK2 enzyme in comparison to CHK1 can be exploited for selectivity.

Having increased potency against the CHK2 enzyme through optimization of the phenol substitution pattern, it was anticipated that this could be combined with additional modification of the pyrrolidine functionality of **10**. From the X-ray of **10**, the 4- or 5-positions of the 3-aminopyrrolidine appeared to offer possible vectors for further substitution. Retaining the 3-(*S*)-aminopyrrolidine chirality optimal in **10**, the diasteroisomeric esters **25** and **26** were made (Table 3). Both showed a reduction in activity, although **26** had improved selectivity against CHK1. Using the methyl ester as a synthetic handle, a range of simple amides were prepared, such as dimethylamide **27**, but no improvement in activity relative to **10** was found. Replacement of the 5-ester by the (1,1-dimethyl)methyl alcohol **28** was also unproductive despite the presence of the potency-enhancing 5-fluorophenol substitution. The simpler methyl alcohol **29** gave only a marginal improvement in activity in comparison to **18**. With no improvements found in selectivity against CHK1 or significant reduction of hERG inhibition, substitution at the pyrrolidine 4-position was investigated instead. The ethyl ester group in **31** was found to be tolerated and was preferred to the enantiomer **30**. Addition of this functionality at the 4-position reduced hERG activity and in the case of **31** gave an improvement in selectivity against CHK1. Given that addition of peripheral polar groups has been identified as a general strategy for reducing hERG activity,[33] the ethyl ester group in **31** was converted to both the methyl and (1,1-dimethyl)methyl alcohols **32** and **33**. In this instance, the more substituted analogue **33** gave a significant improvement in CHK2 activity, as well as retaining high CHK1 selectivity (ca. 120-fold) and maintaining low hERG inhibition.

From the binding of the quinazoline core in the CHK2 enzyme shown by X-ray crystallography (Figure 2), the 6- and 7- positions of the quinazoline presented further opportunity for the addition of groups to enhance both potency and physicochemical properties within the series. A number of mono- and disubstituted quinazolines were therefore synthesized (Table 4). Generally, it was found that a single substitution at the 6-position, such as methoxy **34**, methoxyethoxy **36**, or alcohol **38** analogues, did not improve CHK2 potency. The addition of the peripheral alcohol in **38** was, however, found to reduce hERG activity. Mono substitution at the 7-position was found to give increased CHK2 activity, giving a 2- to 4-fold improvement relative to nonsubstituted compounds. However, substantial hERG inhibition remained, even with the alcohol group present in **39**. Combining substitution at both the 6- and 7-positions was found to be beneficial to both increase CHK2 activity and reduce hERG inhibition, as seen for compounds **40** and **41**. The additive effect on potency of appropriate phenol substitution was demonstrated again by the synthesis of the corresponding fluorophenol analogues **42**, **43**, and **44**, giving compounds active against CHK2 in the 10−30 nM activity range with reduced hERG activity for **44** (hERG IC_{50} = 44 μM). It was also observed that substitution of the quinazoline core at C-6 and/or C-7 had minimal effect on the selectivity for CHK2 over CHK1, as might be anticipated from the orientation of these groups out into solvent.

The various regions of the scaffold had been independently optimized for CHK2 potency, selectivity over CHK1, and reduced hERG inhibition, and it now remained to synthesize the key combinations (Table 5). Combining the 3-pyrazolyl group of **24** and the substituted pyrrolidine of **33** gave the nanomolar CHK2 inhibitor **49**. Selectivity over CHK1 was

Table 3. Modifications to the Pyrrolidine Substituent

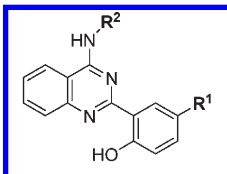

No.	R^1	R^2	CHK2 IC_{50} (μM)[a]	CHK1 IC_{50} (μM)[b]	CHK2/1 selectivity	hERG (inh@10μM)[c]
25	H	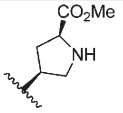	4.6[d]	n.d.[e]	n.d.	n.d.
26	H	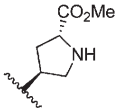	1.05 (0.60, 1.5)	104 (±28)[f]	99	69%
27	H	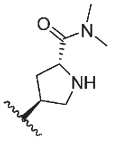	0.181 (±0.044)[f]	20.5 (27, 14)	113	85%
28	F	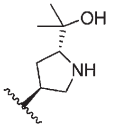	0.46 (0.45, 0.47)	27.5 (25, 30)	60	n.d.
29	F	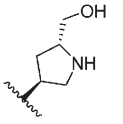	0.081 (±0.025)[f]	1.75 (0.90, 2.6)	22	70%
30	F	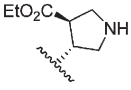	2.85 (2.7, 3.0)	56 (59, 53)	20	30%
31	F	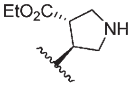	0.154 (±0.026)[f]	28 (31, 25)	182	53%
32	F	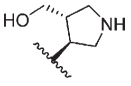	0.037 (0.044, 0.031)	n.d.	n.d.	n.d.
33	F	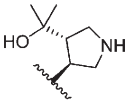	0.021 (0.014, 0.028)	2.6 (1.5, 3.6)	124	25%

[a] Mean of $n = 2$ determinations in DELFIA assay format, individual values in parentheses. Standard inhibitor staurosporine gave mean (±SEM) $IC_{50} = 27$ (±2.6) nM, $n = 10$. [b] Mean of $n = 2$ determinations in DELFIA assay format, individual values in parentheses. Standard inhibitor staurosporine gave mean (±SEM) $IC_{50} = 2.1$ (±0.41) nM, $n = 26$. [c] Mean of multiple determinations ($n = 2-8$) in a high-throughput cell-based electrophysiology assay for inhibition of hERG tail current.[31] DMSO 0.3% aqueous vehicle negative control gave 9−20% inhibition. One μM cisapride positive control gave 89−99% inhibition. [d] Single determination. [e] nd = not determined. [f] Mean (±SEM) for $n = 3$ determinations.

also found to be additive, with near 600-fold selectivity and low hERG activity (**49**, hERG $IC_{50} = 31\ \mu M$). The isomeric pyrazol-4-yl substituted analogue **48** also gave a potent compound with minimal hERG activity, although with somewhat reduced selectivity for CHK2 over CHK1, mirroring the structure−activity seen for **23** and **24**. Potent CHK2 inhibitors were also obtained when combining the (1,1-dimethyl)methyl alcohol substituted pyrrolidines with the 6,7-disubstituted quinazoline core. The 6,7-dimethoxyquinazoline **46** was the most potent CHK2 inhibitor identified in the series, with selectivity (63-fold) over CHK1 and low hERG inhibition (**46**, hERG $IC_{50} = 22\ \mu M$). The 6-methoxy, 7-methoxyethoxy variant **45** gave similar CHK2 and hERG activities, however, it also had lower selectivity over CHK1 (21-fold). The methylene alcohol **47** was found to be a less potent CHK2 inhibitor than **46**, with lower selectivity.

The crystal structure of **46** bound to CHK2 was solved and compared to earlier compounds in the series (Figure 2C).

Table 4. Addition of Solubilizing Groups at C-6 and C-7 of the Quinazoline

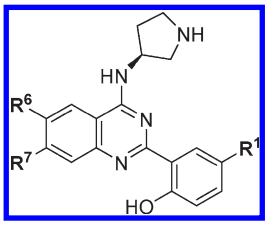

no.	R^1	R^6	R^7	CHK2 IC_{50} (μM)[a]	CHK1 IC_{50} (μM)[b]	CHK2/1 selectivity	hERG (inh@ 10 μM) (%)[c]
34	H	−OMe	−H	0.20 (0.21, 0.19)	nd[d]	nd	nd
35	H	−H	−OMe	0.029 (0.039, 0.019)	0.87 (0.65, 1.08)	30	86
36	H	$-O(CH_2)_2OMe$	−H	0.28 (0.21, 0.35)	5.05 (2.0, 8.1)	18	100
37	H	−H	$-O(CH_2)_2OMe$	0.070 (±0.005)[e]	0.85 (0.90, 0.79)	12	61
38	H	$-(CH_2)_3OH$	−H	0.60 (0.23, 0.97)	26 (±11)[e]	43	28
39	H	−H	$-(CH_2)_3OH$	0.078 (±0.026)[e]	1.1 (1.4, 0.87)	14	77
40	H	−OMe	−OMe	0.028 (0.033, 0.024)	0.87 (±0.30)[e]	31	46
41	H	−OMe	$-O(CH_2)_2OMe$	0.12 (0.042, 0.19)	0.33 (0.32, 0.34)	3	22
42	F	−OMe	−OMe	0.012 (0.015, 0.010)	0.20 (±0.03)[e]	17	68
43	F	−H	$-O(CH_2)_2OMe$	0.011 (0.005, 0.017)	0.14 (0.14, 0.13)	13	65
44	F	−OMe	$-O(CH_2)_2OMe$	0.030 (0.018, 0.043)	0.26 (±0.09)[e]	9	25

[a] Mean of $n = 2$ determinations in DELFIA assay format, individual values in parentheses. Standard inhibitor staurosporine gave mean (±SEM) $IC_{50} = 27$ (±2.6) nM, $n = 10$. [b] Mean of $n = 2$ determinations in DELFIA assay format, individual values in parentheses. Standard inhibitor staurosporine gave mean (±SEM) $IC_{50} = 2.1$ (±0.41) nM, $n = 26$. [c] Mean of multiple determinations ($n = 2-8$) in a high-throughput cell-based electrophysiology assay for inhibition of hERG tail current.[31] DMSO 0.3% aqueous vehicle negative control gave 9−20% inhibition. One μM cisapride positive control gave 89−99% inhibition. [d] nd = not determined. [e] Mean (±SEM) for $n = 3$ determinations.

Overall, the binding mode was found to be very highly conserved relative to previous compounds, with all of the key hydrogen bond interactions maintained. The potency gained with **46** therefore appears to be due to the presence of the two methoxy substituents occupying the solvent exposed region of the enzyme, and contributions from the isopropyl alcohol substituent, which may participate in a second intramolecular hydrogen bond to the quinazoline exocyclic NH in **46**. Although no specific interactions between the alcohol group and enzyme were observed, an increase in order within the glycine-rich P-loop was inferred from the more clearly defined electron density in the crystal structure compared to the complexes of **10** and **24**.

Evaluation of the wider kinase inhibitory profile of the two most potent compounds, **46** and **49**, was undertaken (see Supporting Information).[36] A screen against a total of 85 kinases representative of various branches of the human kinome showed **46** to be the more selective, strongly inhibiting (>90% inhibition @ 1 μM) only 3 of the 85 kinases tested, highlighting PHK and MARK3 along with CHK2. In contrast, **49** was found to be less selective, strongly inhibiting 19 of the 85 enzymes in the panel (>90% inhibition @ 1 μM). This perceived difference in selectivity profile was further supported through calculation of Gini coefficients,[37] taking into account the total inhibitory activities of the compounds across the panel, where **46** gave a value of 0.53, compared to 0.29 for **49**. Interestingly, the selectivity for CHK2 over CHK1 is not representative of a general level of kinase selectivity for this series of compounds.

A qualitative assay for inhibition of CHK2 in HT29 human colon cancer cells was developed based on the ability of the compounds to prevent an electrophoresis gel bandshift of the CHK2 protein following phosphorylation induced by the DNA damaging topoisomerase II inhibitor etoposide. HT29 cells were treated with the CHK2 inhibitor for one hour before addition of etoposide. Inhibition of the bandshift was observed from ca. 1 μM concentration of the inhibitor **46** (Figure 3). Activation of CHK2 in response to DNA damage caused by etoposide was detected by phosphorylation of CHK2 Thr68, regardless of the presence of the CHK2 inhibitor. However, inhibition of CHK2 itself is clearly confirmed by the reduction of the Ser516 autophosphorylation at increasing concentrations of **46**, such that the signal is completely abolished at 1 μM concentration of the compound.

Selected compounds were evaluated for effects in human cancer cells and in vitro pharmacokinetic properties (Table 6). In general, there was a correlation of the concentration at which rescue of etoposide-induced CHK2 bandshift was observed with the potency of the inhibitors in the CHK2 biochemical assay. An exception was **49**, which was apparently less effective in the CHK2 mechanistic assay than anticipated from the in vitro potency. The passive diffusion[38] of these 2-(quinazolin-2-yl)phenols across a membrane of 2% phosphatidylcholine in dodecane was generally assessed as high. Cytotoxicity in HT29 cells was similar for all compounds and did not appear to correlate strongly with inhibition of the etoposide-induced CHK2 bandshift. It is therefore likely that a component of the cytotoxicity is related to off-target effects other than CHK2 inhibition. Some support for this hypothesis is given by the higher cytotoxicity of **49**, despite the apparently weaker inhibitory effects on CHK2 in cells. Interestingly, **49** was significantly less selective than the analogue **46** in the wider kinase selectivity profiling. All the compounds showed good intrinsic metabolic stability when incubated in mouse liver microsomes, which included UDP-glucuronosyltransferase and therefore informed on aspects of both primary and secondary metabolism.[39] The combination of moderate-to-high passive permeability and low intrinsic metabolism indicated promising in vitro pharmacokinetic properties for the compounds.

On the basis of the potency and selectivity of **46** in in vitro and cellular assays, this compound was chosen for

Table 5. Optimal Combinations of Quinazoline, Pyrrolidine, and Phenol Substitution

No.	Structure	CHK2 IC_{50} (μM)[a]	CHK1 IC_{50} (μM)[b]	CHK2/1 selectivity	hERG (inh@ 10μM)[c]
45	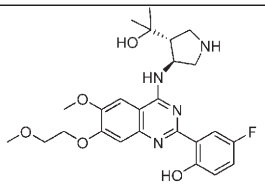	0.005 (0.004, 0.006)	0.105 (0.11, 0.099)	21	16%
46	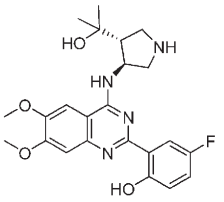	0.003 (0.003, 0.003)	0.19 (0.25, 0.12)	63	17%
47	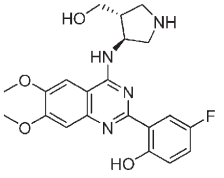	0.011 (0.008, 0.015)	0.23 (0.22, 0.24)	21	n.d.[d]
48	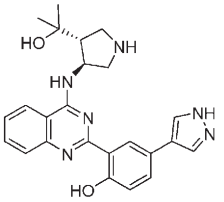	0.014 (0.010, 0.018)	1.7 (1.8, 1.6)	121	9%
49	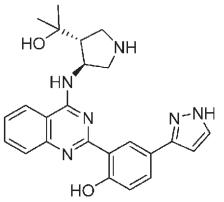	0.008 (±0.002)[e]	4.65 (3.1, 6.2)	581	15%

[a] Mean of $n = 2$ determinations in DELFIA assay format, individual values in parentheses. Standard inhibitor staurosporine gave mean (±SEM) $IC_{50} = 27$ (±2.6) nM, $n = 10$. [b] Mean of $n = 2$ determinations in DELFIA assay format, individual values in parentheses. Standard inhibitor staurosporine gave mean (±SEM) $IC_{50} = 2.1$ (±0.41) nM, $n = 26$. [c] Mean of multiple determinations ($n = 2$−8) in a high-throughput cell-based electrophysiology assay for inhibition of hERG tail current.[31] 0.3% DMSO aqueous vehicle negative control gave 9−20% inhibition. One μM cisapride positive control gave 89−99% inhibition. [d] nd = not determined. [e] Mean (±SEM) of $n = 3$ determinations.

further studies. Radioprotectant effects of CHK2 inhibitors toward nontumorigenic murine and human cells have been reported.[9,18,20,26] Here, isolated mouse thymocytes were incubated with varying concentrations of **46** for an hour before being exposed to ionizing radiation. A protective effect of **46** was indeed observed, in a concentration dependent manner (Figure 4), with complete reduction of radiation-induced apoptosis observed in the presence of 20 μM concentration of **46**.

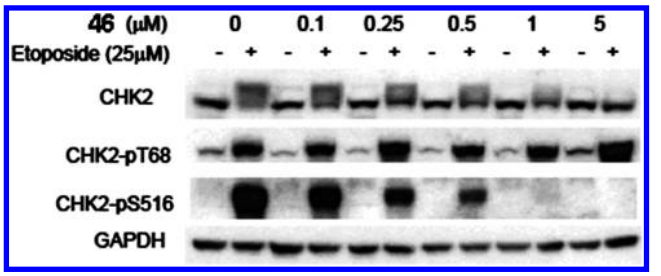

Figure 3. Effect of **46** on CHK2 bandshift and biomarkers for CHK2 activation (CHK2-pT68) and autophosphorylation (CHK-pS516) in HT29 cells. Cells were treated with compound for 1 h followed by 50 μM etoposide for 5 h.

Conclusions

The development of a series of 2-(quinazolin-2-yl)phenols as ATP-competitive CHK2 inhibitors was achieved by stepwise

Table 6. Cellular Activities and in Vitro ADME Properties of Selected Inhibitors

	10	18	43	24	49	46
CHK2 IC_{50} (μM)[a]	0.16	0.060	0.011	0.009	0.008	0.003
CHK2 bandshift MEC (μM)[b]	n.d.[c]	10	5	1	10	1
cytotoxicity in HT29 cells GI_{50} (μM)[d]	1.5	1.8	1.3	0.5	0.3	1.4
maximum passive permeability (Pe) ($\times 10^{-6}$ cm/s)[e]	n.d.	56 (pH 5)	29 (pH 7.4)	37 (pH 6.5)	8 (pH 5)	11 (pH 5)
mouse microsomal turnover (% metabolized at 30 min)[f]	27	25	25	27	22	23

[a] See Tables 1−5. [b] Minimum effective concentration (MEC) for complete inhibition of the etoposide-induced CHK2 bandshift, see footnote to Figure 3. [c] nd = not determined. [d] Single determination using SRB colorimetric assay.[40] [e] Measured at three pH (5, 6.5 and 7.4) in PAMPA.[38] The pH corresponding to maximum permeability is in parentheses. [f] Percent decrease in parent compound as measured by liquid chromatography−mass spectrometry.[39]

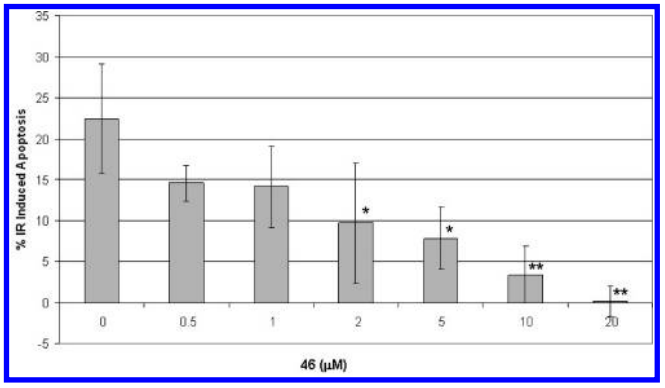

Figure 4. Mouse thymocytes were preincubated for 1 h with indicated doses of **46** before exposure to 5Gy IR. At 16 h post-IR, apoptosis was assessed by Annexin V-FITC FACS. Results shown are mean (±SD) for $n = 3$ determinations. Statistics: * $P < 0.05$ and ** $P < 0.01$ significantly different from no drug control.

optimization of multiple substitutions around the core structure, strongly guided by close analysis of crystal structures of representative compounds bound within the ATP pocket of the CHK2 enzyme. Pleasingly, by combining the separately optimized components around the core quinazoline structure, a generally additive effect with respect to CHK2 potency was observed, resulting in low nanomolar enzyme inhibitors. An early awareness of possible hERG liabilities associated with the 2-(quinazolin-2-yl)phenol scaffold allowed only structural features tending toward reducing hERG activity to be progressed. The addition of polar functionality around the periphery of the core was effective in reducing this off-target activity without detriment to the kinase inhibitory potency. Interestingly, hERG activity was only sensitive to polar substitution at specific positions rather than a reduction being associated with generally increasing polar surface area. Greater than 500-fold selectivity against the related DNA damage response signaling enzyme CHK1 was achieved with pyrazolyl substituents that appear to target differences between the two kinases in the region of the conserved lysine and the C-helix. However, high selectivity for CHK2 inhibition over CHK1 did not predict for high specificity for CHK2 versus a wider selection of protein kinases. Potent CHK2 inhibitors from this series were shown to have favorable in vitro ADME properties, in particular good passive membrane permeability, and the expected inhibition of CHK2 was demonstrated in a mechanistic cell-based assay. Although cytotoxicity toward a human colon cancer cell line in vitro was observed, comparison of the activity of compounds with varying CHK2 target inhibition potencies in cells suggested an off-target component to the antiproliferative effects. Finally, a concentration-dependent radioprotective effect toward mouse thymocytes by the optimized compound **46** was observed. This further confirms the radioprotectant effects of pharmacological inhibition of CHK2 in normal tissue.[18,20,22] These 2-(quinazolin-2-yl)phenol CHK2 inhibitors are potent and selective chemical tool compounds suitable for use in probing the consequences of CHK2 inhibition in cancer cells.[41] In particular, the antiproliferative effect of a combination of the selective small molecule CHK2 inhibitor **46** (CCT241533) with PARP inhibitors will be reported elsewhere.[46]

Experimental Section

Synthetic Chemistry. Synthesis of the requisite quinazolines was achieved by the two general methods outlined in Schemes 1 and 2. The first method used was the reaction of anthranilonitriles with 2-methoxybenzoyl chlorides to give the corresponding amides, which were cyclized under basic conditions to give quinazolines of general structure **50**[28] (Scheme 1). Deprotection of the anisole and displacement of the 4-chloro substituent with an appropriate amine provided the desired targets **51**. This route is exemplified in Scheme 1 by the synthesis of **49**, where subsequent modification of the phenol group to install a pyrazole by a Suzuki−Miyaura reaction was also carried out.

An alternative general method is shown in Scheme 2. Quinazoline-2,4-diones **55**, either commercially available or synthesized from the relevant 2-nitroesters,[43] were activated by reaction with phosphorus oxychloride. Selective displacement by amines at the 4-position followed by Suzuki−Miyaura coupling provided the desired compounds **57**. The synthesis of **46** from 6,7-dimethoxyquinazolin-2,4-dione is shown as a specific example. The particular method used to synthesize the quinazoline cores for all compounds and details of further structural elaborations are described in the Supporting Information.

General Experimental. Starting materials and solvents were purchased from commercial suppliers and were used without further purification. Microwave reactions were carried out in a Biotage Initiator 60 microwave reactor. Organic solutions were dried over $MgSO_4$ or Na_2SO_4. Flash silica chromatography was performed using Merck silica gel 60 (0.025−0.04 mm). Ion exchange chromatography was performed using Isolute Flash SCX-II (acidic) or Flash NH2 (basic) resin cartridges. Automated MPLC was performed on a Biotage SP1 Instrument using prepacked silica cartridges and UV-triggered fraction collection (254 nm). ^{1}H NMR spectra were recorded on a Bruker AMX500 instrument using an internal deuterium lock. ^{13}C NMR spectra were recorded on a Bruker AMX500 instrument at 126 MHz using an internal deuterium lock. Chemical shifts (δ) are referenced to the solvent in which they were measured. GC-MS analyses were performed on a Thermo Trace/Finnigan Polaris Q system with a Zebron 15 m × 0.25 mm i.d. column with 2.5 μm film thickness using helium as the carrier gas at a flow rate of 1.8 mL/min and measuring the sample mass following ionization by EI or CI. Combined HPLC-MS analyses were recorded using a Waters Alliance 2795 separations module and Waters/Micromass LCT mass detector with electrospray ionization (+ve or −ve ion mode as indicated) and with HPLC performed using Phenomenex Gemini C18, 50 mm × 4.6 mm

Scheme 1[a]

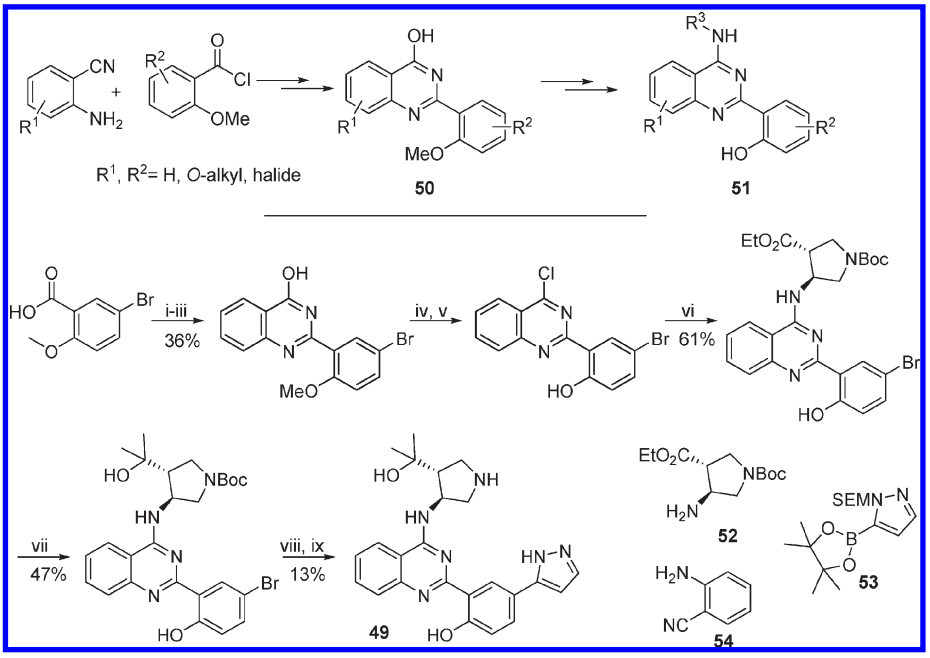

[a] Reagents and conditions: (i) $S(O)Cl_2$; (ii) **54**, Hunigs base, $CHCl_3$; (iii) 20% w/v aq NaOH, H_2O_2; (iv) $P(O)Cl_3$; (v) BBr_3, CH_2Cl_2; (vi) **52**,[42] Et_3N, CH_2Cl_2; (vii) MeMgBr, THF; (viii) **53**, $Pd(PPh_3)_4$, K_3PO_4, DMA, H_2O; (ix) 4 M HCl in dioxane, MeOH.

Scheme 2[a]

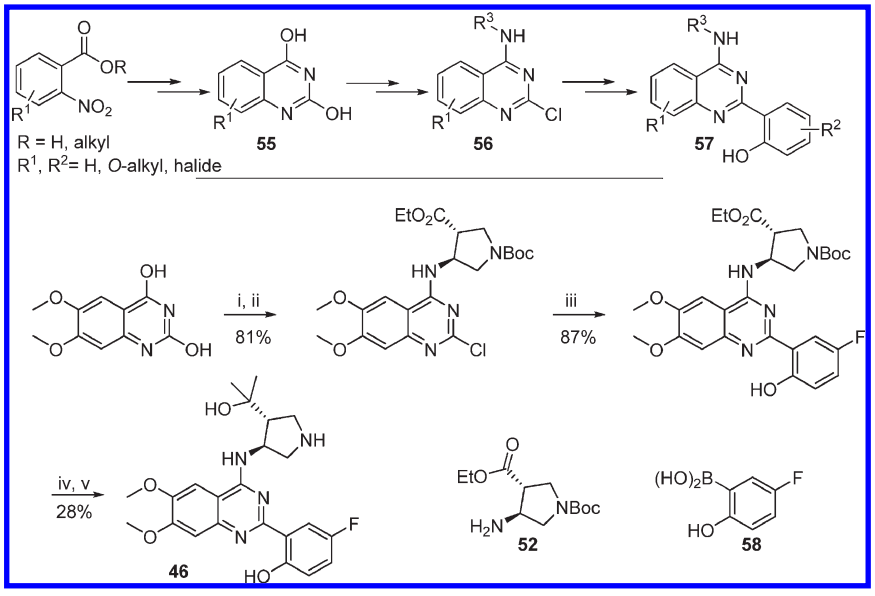

[a] Reagents and conditions: (i) $P(O)Cl_3$, reflux; (ii) **52**,[42] Et_3N, CH_2Cl_2, reflux; (iii) **58**, $Pd(PPh_3)_4$, Na_2CO_3, toluene, H_2O; (iv) MeMgBr, THF; (v) 4 M HCl in dioxane, MeOH.

or 30 mm × 4.6 mm i.d. columns, at a temperature of 22 °C with gradient elution of 10−90% MeOH/0.1% aqueous formic acid at a flow rate of 1 mL/min and a run time of 3.5, 6, or 10 min as indicated. Compounds were detected at 254 nm using a Waters 2487 dual absorbance detector. All tested compounds gave >95% purity as determined by this method.

4-Fluoro-2-(4-((3*S*,4*R*)-4-(2-hydroxypropan-2-yl)pyrrolidin-3-ylamino)-6,7-dimethoxyquinazolin-2-yl)phenol (46). A solution of 6,7-dimethoxyquinazoline-2,4-diol (1.000 g, 4.500 mmol) in $P(O)Cl_3$ (20 mL) was refluxed for 14 h. The reaction mixture was concentrated and dissolved in CH_2Cl_2 (200 mL). The organic phase was washed with iced H_2O (100 mL) and brine (100 mL) and then concentrated to give crude 2,4-dichloro-6,7-dimethoxyquinazoline. The crude material was dissolved in CH_2Cl_2 (14 mL), (3*R*,4*S*)-1-*tert*-butyl 3-ethyl 4-aminopyrrolidine-1,3-dicarboxylate hydrochloride (0.900 g, 3.053 mmol),[42] and Et_3N (1.7 mL, 12.273 mmol) added and the resulting solution refluxed for 4 days. The reaction was cooled, H_2O (100 mL) added, and the aqueous extracted with CH_2Cl_2 (2 × 100 mL). Organic layers were combined, dried over $MgSO_4$, and the crude product purified by silica column chromatography (67% EtOAc in hexanes) to give (3*R*,4*S*)-1-*tert*-butyl 3-ethyl 4-(2-chloro-6,7-dimethoxyquinazolin-4-ylamino)pyrrolidine-1,3-dicarboxylate (1.189 g, 81%). LC-MS (3.5 min) *m*/*z* 481, 483 [M + H^+], R_t 2.69 min. ^1H NMR (500 MHz, $CDCl_3$) δ 7.17 (s, 1H), 6.91 (s, 1H), 5.90 (br d, J = 6.5 Hz, 1H), 5.06 (pent, J = 6.5 Hz, 1H),4.22

(q, J = 7.0 Hz, 1H), 4.13−4.06 (m, 1H), 4.01 (s, 3H), 3.99 (s, 3H), 3.87−3.69 (m, 2H), 3.51−3.31 (m, 1H), 3.25−3.18 (m, 1H), 1.50 (s, 9H), 1.25 (t, J = 7.0 Hz, 1H). (3*R*,4*S*)-1-*tert*-Butyl 3-ethyl 4-(2-chloro-6,7-dimethoxyquinazolin-4-ylamino)pyrrolidine-1,3-dicarboxylate (0.962 g, 2.000 mmol), 5-fluoro-2-hydroxyphenylboronic acid (0.344 g, 2.200 mmol), Na_2CO_3 (0.636 g, 6.000 mmol), and $Pd(PPh_3)_4$ (0.114 g, 0.100 mmol) were dissolved in toluene (5 mL) and H_2O (2 mL) and N_2 bubbled through the resulting biphasic mixture for 30 min. The mixture was then heated at 100 °C for 24 h. The mixture was cooled and H_2O (100 mL) added. The aqueous layer was extracted with EtOAc (2 × 100 mL). Organic extracts were combined, dried over $MgSO_4$, and concentrated. Purification by silica column chromatography (67% EtOAc in hexanes) gave (3*R*,4*S*)-1-*tert*-butyl 3-ethyl 4-(2-(5-fluoro-2-hydroxyphenyl)-6,7-dimethoxyquinazolin-4-ylamino)pyrrolidine-1,3-dicarboxylate (0.969 g, 87%). LC-MS (3.5 min) m/z 557 [M + H^+], R_t 2.97 min. ^{1}H NMR (500 MHz, $CDCl_3$) δ 8.20 (dd, J = 10.0, 3.0 Hz, 1H), 7.20−7.15 (m, 1H), 7.10−7.02 (m, 2H), 6.95 (dd, J = 9.0, 4.5 Hz, 1H), 6.34 (br d, J = 5.0 Hz, 1H), 5.17−5.12 (m, 1H), 4.32−4.26 (m, 2H), 4.03 (s, 3H), 4.02 (s, 3H), 3.94−3.32 (m, 5H), 1.52 (s, 9H), 1.28 (t, J = 7.0 Hz, 1H). MeMgBr (5.7 mL of a 3 M solution in Et_2O) was added to a solution of (3*R*,4*S*)-1-*tert*-butyl 3-ethyl 4-(2-(5-fluoro-2-hydroxyphenyl)-6,7-dimethoxyquinazolin-4-ylamino)pyrrolidine-1,3-dicarboxylate (0.969 g, 1.723 mmol) in THF (17 mL) at 0 °C. After 1 h at rt, satd aq NH_4Cl (100 mL) was carefully added and the aqueous layer extracted with EtOAc (2 × 75 mL). The organic layer was dried, concentrated, and the resulting crude material resubjected to the above reaction conditions due to presence of unreacted SM and intermediate methyl ketone. The resulting crude was purified by silica column chromatography (EtOAc) and the isolated Boc protected amine stirred in a solution of MeOH (20 mL) and HCl (10 mL of a 4 M solution in dioxane) for 24 h. The reaction was concentrated, and the resulting crude product purified by SCX-2 Isolute column, washing first with MeOH and finally with 1 M NH_3 in MeOH. Purification by Biotage column chromatography (silica KP-NH, 5% MeOH in CH_2Cl_2) gave 4-fluoro-2-(4-((3*S*,4*R*)-4-(2-hydroxypropan-2-yl)pyrrolidin-3-ylamino)-6,7-dimethoxyquinazolin-2-yl)phenol **46** (0.212 g, 28%). LC-MS (3.5 min) m/z 355 [M + H^+], R_t 1.92 min. ^{1}H NMR (500 MHz, MeOD) δ 8.13 (dd, J = 10.0, 3.0 Hz, 1H), 7.51 (s, 1H), 7.09 (s, 1H), 7.03 (ddd, J = 9.0, 8.0, 3.0 Hz, 1H), 6.86 (dd, J = 9.0, 4.5 Hz, 1H), 5.06−5.02 (m, 1H), 3.98 (s, 3H), 3.97 (s, 3H), 3.40−3.25 (m, 2H), 3.05−2.94 (m, 2H), 2.46 (dd, J = 14.0, 8.0 Hz, 1H), 1.32 (s, 3H), 1.30 (s, 3H). ^{13}C NMR (126 MHz, DMSO) δ 158.1, 157.2, 156.7, 154.6 (d, J = 233 Hz), 154.5, 148.8, 143.4, 120.0 (d, J = 8 Hz), 118.6 (d, J = 24 Hz), 118.3 (d, J = 8 Hz), 113.6 (d, J = 8 Hz), 107.0, 106.2, 102.7, 69.5, 56.3, 55.9, 55.6, 54.5, 53.6, 48.1, 28.6, 28.1 HRMS calcd for $C_{22}H_{27}N_4O_4F$ (M + H^+) 443.2089, found 443.2096.

Acknowledgment. We thank Dr. A. Mirza, Dr. M. Liu, and G. M. Richards for assistance in the characterization of test compounds. We thank Dr. T. P. Matthews for assistance in arranging hERG assays. This work was supported by Cancer Research UK [CUK] grant numbers C309/A2187, C309/A2874, C309/A8365, and C302/A8265 and Infrastructure Support grant C302/A7803 and by the Institute of Cancer Research. We acknowledge NHS funding to the NIHR Biomedical Research Centre.

Supporting Information Available: Experimental conditions for CHK2 and CHK1 DELFIA. Experimental conditions for SRB cytotoxicity assay in HT29 cells. Preparation and characterization data for compounds **5**−**45**, **47**−**49**. Kinase selectivity data for compounds **46** and **49**. Experimental procedure for the determination of inhibitor-CHK2 crystal structures and statistics for the data collection and refinement of complexes of CHK2 with **10**, **24**, and **46**. Experimental method for radioprotectant studies of **46** in mouse thymocytes. Alignment analysis of CHK1 and CHK2 sequences. Analysis of CHK1 and CHK2 binding sites. This material is available free of charge via the Internet at http://pubs.acs.org.

References

(1) Lengauer, C.; Kinzler, K. W.; Vogelstein, B. Genetic Instabilities in Human Cancers. *Nature* **1998**, *396*, 643–649.
(2) Coleman, W. B.; Tsongalis, G. J. The Role of Genomic Instability in Human Carcinogenesis. *Anticancer Res.* **1999**, *19*, 4645–4664.
(3) Reinhardt, H.; Yaffe, M. Kinases that Control the Cell Cycle Response to DNA damage: Chk1, Chk2, and MK2. *Curr. Opin. Cell Biol.* **2009**, *21*, 245–255.
(4) Samuel, T.; Weber, H.; Funk, J. Linking DNA Damage to Cell Cycle Checkpoints. *Cell Cycle* **2002**, *2*, 162–168.
(5) Stracker, T. H.; Usui, T.; Petrini, J. H. Taking the time to make important decisions: the checkpoint effector kinases Chk1 and Chk2 and the DNA damage response. *DNA Repair* **2009**, *8*, 1047–1054.
(6) Antoni, L.; Sodha, N.; Collins, I.; Garrett, M. D. CHK2 kinase: cancer susceptibility and cancer therapy—two sides of the same coin? *Nature Rev. Cancer* **2007**, *7*, 925–936.
(7) Kastan, M. B.; Bartek, J. Cell-cycle checkpoints and cancer. *Nature* **2004**, *432*, 316–323.
(8) Bartek, J.; Lukas, J. Chk1 and Chk2 kinases in checkpoint control and cancer. *Cancer Cell* **2003**, *3*, 421–429.
(9) Hirao, A.; Kong, Y.; Matsuoka, S.; Wakeman, A.; Ruland, J.; Yoshida, H.; Liu, D.; Elledge, S.; Mak, T. DNA Damage-Induced Activation of p53 by the Checkpoint Kinase Chk2. *Science* **2000**, *287*, 1824–1827.
(10) Ahn, J. Y.; Schwarz, J. K.; Piwnica-Worms, H.; Canman, C. E. Phosphorylation of threonine 68 promotes oligomerization and autophosphorylation of the Chk2 protein kinase via the forkhead-associated domain. *Cancer Res.* **2000**, *60*, 5934–5936.
(11) Matsuoka, S.; Rotman, G.; Ogawa, A.; Shiloh, Y.; Tamai, K.; Elledge, S. Ataxia telangiectasia-mutated phosphorylates Chk2 in vivo and in vitro. *Proc. Natl. Acad. Sci. U.S.A.* **2000**, *97*, 10389–10394.
(12) Ahn, J.; Li, X.; Davis, H. L.; Canman, C. E. Phosphorylation of threonine 68 promotes oligomerization and autophosphorylation of the Chk2 protein kinase via the forkhead-associated domain. *J. Biol. Chem.* **2002**, *277*, 19389–19395.
(13) Oliver, A. W.; Paul, A.; Boxall, K. J.; Barrie, S. E.; Aherne, G. W.; Garrett, M. D.; Mittnacht, S.; Pearl, L. H. Trans-activation of the DNA-damage signalling protein kinase Chk2 by T-loop exchange. *EMBO J.* **2006**, *25*, 3179–3190.
(14) Wu, X.; Chen, J. Autophosphorylation of checkpoint kinase 2 at serine 516 is required for radiation-induced apoptosis. *J. Biol. Chem.* **2003**, *278*, 36163–36168.
(15) Schwarz, J. K.; Lovly, C. M.; Piwnica-Worms, H. Regulation of the Chk2 protein kinase by oligomerization-mediated cis- and trans-phosphorylation. *Mol. Cancer Res.* **2003**, *1*, 598–609.
(16) Pommier, Y.; Sordet, O.; Rao, V. A.; Zhang, H.; Kohn, K. W. Targeting chk2 kinase: molecular interaction maps and therapeutic rationale. *Curr. Pharm. Des.* **2005**, *11*, 2855–2872.
(17) Pommier, Y.; Weinstein, J. N.; Aladjem, M. I.; Kohn, K. W. Chk2 molecular interaction map and rationale for Chk2 inhibitors. *Clin. Cancer Res.* **2006**, *12*, 2657–2661.
(18) Arienti, K. L.; Brunmark, A.; Axe, F. U.; McClure, K.; Lee, A.; Blevitt, J.; Neff, D. K.; Huang, L.; Crawford, S.; Pandit, C. R.; Karlsson, L.; Breitenbucher, J. G. Checkpoint kinase inhibitors: SAR and radioprotective properties of a series of 2-arylbenzimidazoles. *J. Med. Chem.* **2005**, *48*, 1873–1885.
(19) McClure, K. J.; Huang, L.; Arienti, K. L.; Axe, F. U.; Brunmark, A.; Blevitt, J.; Breitenbucher, J. G. Novel non-benzimidazole chk2 kinase inhibitors. *Bioorg. Med. Chem. Lett.* **2006**, *16*, 1924–1928.
(20) Carlessi, L.; Buscemi, G.; Larson, G.; Hong, Z.; Wu, J. Z.; Delia, D. Biochemical and cellular characterization of VRX0466617, a novel and selective inhibitor for the checkpoint kinase Chk2. *Mol. Cancer Ther.* **2007**, *6*, 935–944.
(21) Larson, G.; Yan, S.; Chen, H.; Rong, F.; Hong, Z.; Wu, J. Z. Identification of novel, selective and potent Chk2 inhibitors. *Bioorg. Med. Chem. Lett.* **2007**, *17*, 172–175.
(22) Jobson, A. G.; Cardellina, J. H.; Scudiero, D.; Kondapaka, S.; Zhang, H.; Kim, H.; Shoemaker, R.; Pommier, Y. Identification of a Bis-guanylhydrazone [4,4′-Diacetyldiphenylurea-bis(guanylhydrazone); NSC 109555] as a novel chemotype for inhibition of Chk2 kinase. *Mol. Pharmacol.* **2007**, *72*, 876–884.
(23) Hilton, S.; Naud, S.; Caldwell, J. J.; Boxall, K.; Burns, S.; Anderson, V. E.; Antoni, L.; Allen, C. E.; Pearl, L. H.; Oliver, A. W.; Aherne, G. W.; Garrett, M. D.; Collins, I. Identification and characterisation of 2-aminopyridine inhibitors of checkpoint kinase 2. *Bioorg. Med. Chem.* **2010**, *18*, 707–718.

(24) Levesque, A.; Eastman, A. p53-Based Cancer Therapies: Is Defective p53 the Achilles Heel of the tumor? *Carcinogenesis* **2007**, *28*, 13–20.
(25) Kruse, J-. P.; Gu, W. Modes of p53 Regulation. *Cell* **2009**, *137*, 609–622.
(26) Takai, H.; Naka, K.; Okada, Y.; Watanabe, M.; Harada, N.; Saito, S.; Anderson, C. W.; Appella, E.; Nakanishi, M.; Suzuki, H.; Nagashima, K.; Sawa, H.; Ikeda, K.; Motoyama, N. Chk2-deficient mice exhibit radioresistance and defective p53-mediated transcription. *EMBO J*. **2002**, *21*, 5195–5205.
(27) Jobson, A. G.; Lountos, G. T.; Lorenzi, P. L.; Llamas, J.; Connelly, J.; Cerna, D.; Tropea, J. E.; Onda, A.; Zoppoli, G.; Kondapaka, S.; Zhang, G.; Caplen, N. J.; Cardellina, J. H.; Yoo, S. S.; Monks, A.; Self, C.; Waugh, D. S.; Shoemaker, R. H.; Pommier, Y. Cellular inhibition of checkpoint kinase 2 (Chk2) and potentiation of camptothecins and radiation by the novel Chk2 inhibitor PV1019 [7-nitro-1*H*-indole-2-carboxylic acid {4-[1-(guanidinohydrazone)-ethyl]-phenyl}-amide]. *J. Pharmacol. Exp. Ther*. **2009**, *331*, 816–826.
(28) Raynham, T. M.; Hammonds, T. R.; Gilliatt, J. H.; Charles, M. D.; Pave, G. A.; Foxton, C. H.; Carr, J. L.; Mistry, N. S. Aminoethylamino-aryl (AEAA) compounds as PKD inhibitors and their preparation, pharmaceutical compositions and use in the treatment of PKD-mediated diseases. PCT Int. Appl. WO2007125331, 2007.
(29) Collins, I.; Caldwell, J. J.; Oliver, A. W.; Raynham, T. M.; Welsh, E. J.; Matijssen, C. A. Preparation of oxy-phenyl-aryl compounds as CHK2 kinase inhibitors for treating proliferative disorders and for radioprotection. PCT Int. Appl. WO2009053694, 2009.
(30) Harikumar, K. B.; Kunnumakkara, A. B.; Ochi, N.; Tong, Z.; Deorukhkar, A.; Sung, B.; Kelland, L.; Jamieson, S.; Sutherland, R.; Raynham, T.; Charles, M.; Bagherazadeh, A.; Foxton, C.; Boakes, A.; Farooq, M.; Maru, D.; Diagaradjane, P.; Matsuo, Y.; Sinnett-Smith, J.; Gelovani, J.; Krishnan, S.; Aggarwal, B. B.; Rozengurt, E.; Ireson, C. R.; Guha, S. A novel small-molecule inhibitor of protein kinase D blocks pancreatic cancer growth in vitro and in vivo. *Mol. Cancer Ther*. **2010**, *9*, 1136–1146.
(31) *Ion Channel CardiacProfiler*; Millipore Corporation: Billerica, MA; http://www.millipore.com/drugdiscovery/dd3/ionchannelprofiler.
(32) Wilson, D.; Fanning, L. T. D.; Krenitsky, P.; Termin, A.; Joshi, P.; Sheth, U. Quinazolines useful as modulators of voltage gated ion channels and their preparation, pharmaceutical compositions and use in the treatment of diseases. PCT Int. Appl. WO2007058989, 2007.
(33) Jamieson, C.; Moir, E. M.; Rankovic, Z.; Wishart, G. Medicinal chemistry of hERG optimizations: highlights and hang-ups. *J. Med. Chem*. **2006**, *49*, 5029–5046.
(34) Berman, H. M.; Westbrook, J.; Feng, Z.; Gilliland, G.; Bhat, T. N.; Weissig, H.; Shindyalov, I. N.; Bourne, P. E. The Protein Data Bank. *Nucleic Acids Res*. **2000**, *28*, 235–242.
(35) DeLano, W. L. *The PyMOL Molecular Graphics System*, 2009.
(36) *The National Centre for Protein Kinase Profiling, MRC Protein Phosphorylation Unit, Dundee University*; http://www.kinase-screen.mrc.ac.uk/
(37) Graczyk, P. P. Gini coefficient: a new way to express selectivity of kinase inhibitors against a family of kinases. *J. Med. Chem*. **2007**, *50*, 5773–5779.
(38) Kansy, M.; Senner, F.; Gubernator, K. Physicochemical high throughput screening: parallel artificial membrane permeation assay in the description of passive absorption processes. *J. Med. Chem*. **1998**, *41*, 1007–1010.
(39) Di, L.; Kerns, E. H.; Hong, Y.; Kleintop, T. A.; McConnell, O. J.; Huryn, D. M. Optimization of a higher throughput microsomal stability screening assay for profiling drug discovery candidates. *J. Biomol. Screening* **2003**, *8*, 453–462.
(40) Skehan, P.; Storeng, R.; Scudiero, D.; Monks, A.; McMahon, J.; Vistica, D.; Warren, J. T.; Bokesch, H.; Kenney, S.; Boyd, M. R. New colorimetric cytotoxicity assay for anticancer-drug screening. *J. Natl. Cancer Inst*. **1990**, *82*, 1107–1112.
(41) Workman, P.; Collins, I. Probing the probes: fitness factors for small molecule tools. *Chem. Biol*. **2010**, *17*, 561–577.
(42) Simpson, G. L.; Gordon, A. H.; Lindsay, D. M.; Promsawan, N.; Crump, M. P.; Mulholland, K.; Hayter, B. R.; Gallagher, T. Glycosylated Foldamers to Probe the Carbohydrate−Carbohydrate Interaction. *J. Am. Chem. Soc*. **2006**, *128*, 10638–10639.
(43) Feng, J.; Zhang, Z.; Wallace, M. B.; Stafford, J. A.; Kaldor, S. W.; Kassel, D. B.; Navre, M.; Shi, L.; Skene, R. J.; Asakawa, T.; Takeuchi, K.; Xu, R.; Webb, D. R.; Gwaltney, S. L. Discovery of Alogliptin: A Potent, Selective, Bioavailable, and Efficacious Inhibitor of Dipeptidyl Peptidase IV. *J. Med. Chem*. **2007**, *50*, 2297–2300.
(44) Potterson, L.; McNicholas, S.; Krissinel, E.; Gruber, J.; Cowtan, K.; Emsley, P.; Murshudov, G. N.; Cohen, S.; Perrakis, A.; Noble, M. Developments in the CCP4Molecular-Graphics Project. *Acta Crystallogr., Sect. D: Biol. Crystallogr*. **2004**, *60*, 2288–2294.
(45) McCabe, N.; Turner, N. C.; Lord, C. J.; Kluzek, K.; Bialkowska, A.; Swift, S.; Giavara, S.; O'Connor, M. J.; Tutt, A. N.; Zdzienicka, M. Z.; Smith, G. C. M.; Ashworth, A. Deficiency in the repair of DNA damage by homologous recombination and sensitivity to poly(ADP-ribose) polymerase inhibition. *Cancer Res*. **2006**, *66*, 8109–8115.
(46) Anderson, V. E.; Walton, M. I.; Eve, P. D.; Caldwell, J. J.; Pearl, L. H.; Oliver, A. W.; Collins, I.; Garrett. M. D. CCT241533 is a potent and selective inhibitor of CHK2 which potentiates the cytotoxicity of PARP inhibitors. *Cancer Res*. **2010**; *70*, manuscript accepted for publication.
(47) Matthews, T. P.; McHardy, T.; Klair, S.; Boxall, K.; Fisher, M.; Cherry, M.; Allen, C. E.; Addison, G. J.; Ellard, J.; Aherne, G. W.; Westwood, I. M.; van Montfort, R.; Garrett, M. D.; Reader, J. C.; Collins, I. Design and evaluation of 3,6-di(hetero)aryl imidazo-[1,2-*a*]pyrazines as inhibitors of checkpoint and other kinases. *Bioorg. Med. Chem. Lett*. **2010**, *20*, 4045–4049.